Research Square

Preprints are preliminary reports that have not undergone peer review.
They should not be considered conclusive, used to inform clinical practice,
or referenced by the media as validated information.

Balancing Protein Expression and Minicell Yield in E. coliNissle 1917 via RBS Engineering

Yao Ruan
Xi'an International Medical Center Hospital Affliated to Northwest University
Honglei Xie
First Affiliated Hospital of Xi'an Jiaotong University
Yan Niu
Xi'an International Medical Center Hospital Affliated to Northwest University
Tian Liu
Xi'an International Medical Center Hospital Affliated to Northwest University
Xi Shen
Xi'an International Medical Center Hospital Affliated to Northwest University
Mingxia Zhang
Xi'an International Medical Center Hospital Affliated to Northwest University
Shengping Lei
Xi'an International Medical Center Hospital Affliated to Northwest University
Jun Yu
pclamper@163.com

Xi'an International Medical Center Hospital Affliated to Northwest University

Research Article

Keywords: minicell, ribosome-binding site, target protein, Escherichia coli Nissle 1917

Posted Date: August 29th, 2026

DOI: https://doi.org/10.21203/rs.3.rs-10573832/v1

License: This work is licensed under a Creative Commons Attribution 4.0 International License.
Read Full License

Additional Declarations: No competing interests reported.

Abstract

Background

Bacterial minicells represent promising platforms for targeted drug delivery and enzymatic bioreactors. However, the relationship between recombinant protein expression and minicell production remains unclear, and strategies to simultaneously optimize both minicell yield and the quality of the expressed protein remain to be developed.

Results

An engineered minicell-producing strain (ΔEcN) was constructed from *Escherichia coli* Nissle 1917. To precisely modulate protein expression, the native ribosome-binding site (RBS) upstream of enhanced green fluorescent protein (eGFP) in the plasmid pUC19-eGFP was replaced with two RBS variants (OmpA-RBS and J61100-RBS) of different strengths. The resulting plasmids were individually transformed into ΔEcN. In this strain, RBS engineering generated a gradient of eGFP expression levels (Lac-eGFP > J61100-eGFP > OmpA-eGFP). Higher eGFP expression was correlated with a significant reduction in minicell yield, suggesting a metabolic burden. Notably, while higher expression of eGFP in whole cells was associated with lower solubility, the solubilities of Lac-eGFP and J61100-eGFP were markedly greater within purified minicells than in parental bacteria. Despite the observed differences in minicell yield, integrity remained consistent across all groups, and the hierarchical expression pattern imposed by the RBS variants was faithfully preserved in the minicells.

Conclusions

This study demonstrated that RBS strength can serve as a critical determinant for balancing the recombinant protein load and minicell yield. Furthermore, the finding that minicells provide a superior environment for the soluble accumulation of proteins of interest highlights their advantages as a production platform. In summary, this study establishes a rational technology platform for designing minicell-based systems, where RBS optimization can be used to concurrently maximize functional protein encapsulation and nanoparticle output for therapeutic and biocatalytic applications.

Background

The convergence of nanotechnology and biotechnology has driven the development of delivery systems for biomedical applications [1–3]. Significant research efforts are currently being devoted to developing more personalized and advanced nanocarrier systems [4]. However, conventional Conventional synthetic nanocarriers often face limitations such as poor biocompatibility, complex manufacturing processes, and potential immunogenicity [5, 6]. Therefore, there is a pressing need to explore next-generation nanocarriers that can effectively overcome these challenges.

Bacterial minicells, which are nanoscale vesicles formed through asymmetric cell division in the polar regions of rod-shaped bacteria, have emerged as highly promising natural candidates for use in nanocarrier applications [7–9]. A key advantage of minicells over conventional synthetic nanoparticles lies in their biological origin, which allows the efficient loading of proteins, nucleic acids and small molecules via intrinsic cellular machinery [10, 11]. Minicells lack chromosomal DNA, preventing replication and eliminating pathogenic potential[12]. This characteristic effectively mitigates a primary biosafety concern inherent to bacterial-based systems. Additionally, minicells retain essential metabolic components from their parental bacteria, particularly ribosomes and energy-generating systems. These features allow stable expression of exogenous plasmid DNA and facilitate straightforward genetic modification [13–15]. In particular, minicells derived from the representative probiotic strain *Escherichia coli* Nissle 1917 (EcN) possess essential characteristics including low immunogenicity, high drug-loading capacity, and excellent biocompatibility [16–18]. They also present additional advantages, including specific immunomodulatory functions and the ability to colonize tumor sites [15, 19, 20]. Consequently, EcN-derived minicells represent one of the most promising natural nanocarriers for biomedical applications.

Despite these superior features, a critical barrier to the translational development of minicell-based systems remains: the relationship between the quality of target protein in the parent bacterium and the yield of the resulting minicells. While high-level expression of heterologous proteins is often essential for conferring therapeutic or targeting functions, it may also impose a metabolic burden that compromises bacterial growth, division, and ultimately minicell biogenesis[21]. Conversely, insufficient protein expression may limit the functional efficacy of the assembled minicells. Thus, achieving an optimal balance between protein loading and nanoparticle production is a fundamental challenge in the rational design of engineered minicells.

Current strategies for controlling protein expression in bacteria largely rely on promoter engineering. However, this approach primarily regulates transcription and may not provide the fine-tuning required at the translational level [22]. The ribosome-binding site (RBS), which governs translation initiation efficiency, offers a more direct and modular means to precisely adjust protein output without altering transcriptional regulation[23–25]. Although RBS engineering has been widely adopted in synthetic biology and metabolic engineering, its application to optimize the concurrent production of functional proteins and minicells has not yet been systematically explored.

Therefore, this study aims to precisely regulate the expression of a model protein, enhanced green fluorescent protein (eGFP), in an EcN-derived minicell-producing strain via RBS variants. We seek to elucidate the effects of RBS engineering on protein solubility, cellular integrity, and crucially, the yield and protein content of harvested minicells. By establishing a quantitative framework that links RBS strength to minicell production and functionality, this study intends to provide a rational design principle for developing next-generation minicell platforms optimized for both high therapeutic protein loading and efficient nanoparticle assembly.

Methods

Preparation of minicells from ΔEcN

The bacterial strains used in this study are listed in Table 1. To facilitate the production of minicells, the *minCD* gene cluster (*minC* and *minD*, Table 1)[26] in the EcN genome was knocked out using λ Red homologous recombination [27,28]. Briefly, the kanamycin (Kan) resistance gene with two flipase recognition target (FRT) sites was cloned from the pKD13 plasmid via nested polymerase chain reaction (PCR) using two pairs of primers (KT-F1/KT-R1 and KT-F2/KT-R2) [29]. Its upstream and downstream regions are homologous to the terminal regions of the *minCD* gene. The pure PCR products were then collected and transferred to EcN cells with the Red recombinase pKD46 plasmid to conduct homologous recombination. The derived strains were cultured on LB agar plates containing kanamycin (50 μg/mL) at 42°C to remove the pKD46 plasmid. The EcN strain lacking the *minCD* gene (ΔEcN) was subsequently obtained. The DNA fragments lacking the *minCD* gene were PCR-amplified using primers ID-F and ID-R for agarose gel electrophoresis and sequencing. The gene sequence of the primers used in the study are listed in the Supplementary Material (Table S1). The synthesis of primers and the sequencing of genes were carried out by Convenience Biology Corporation (Changzhou, China). The morphology of the ΔEcN strain and the budding state of the minicell were captured via a biological microscope (Leica DM3000, Wetzlar, Germany) with hematoxylin–eosin (HE) staining. The growth curves of EcN and ΔEcN were drawn to assess the growth status.

Table 1 | Key strains, plasmids and genes used in this study.

Strain/plasmid/gene	Genotype or description	Reference or source	GenBank accession No. or Gene ID No.
Strains			
EcN	*Escherichia coli Nissle* 1917, O6:K5:H1	Biobw (Beijing)	NZ_CP022686
ΔEcN	EcNΔ*minCD*::*kan*, Kan^R	This study	
Plasmids			
pKD13	Template plasmid, suicide vector, Amp^R , Kan^R	This laboratory	AY048744.1
pKD46	Red recombinase plasmid, temperature sensitive, Amp^R	This laboratory	MF287367.1
pUC19-eGFP	includes *eGFP*, *lac promoter*,Amp^R	Genecarer (Xi'an)	
pUC19-OmpA-eGFP	includes OmpA rbs-eGFP, Amp^R	This study	
pUC19-J61100-eGFP	includes J61100 rbs-eGFP, Amp^R	This study	
Genes			
minC	Z-ring positioning protein MinC		945744
minD	Z-ring positioning protein MinD		945741

Purification and characterization of minicells

The ΔEcN cells were grown in 10 mL of LB liquid medium supplemented with 50 μg/mL kanamycin at 37°C and 220 rpm. An overnight culture was transferred at 1% (v/v) into 1 L of fresh medium, and shaken at 220 rpm at 37°C until the OD_{600} reached 0.6–0.8. Then, 1 mL of the culture was centrifuged at 13000 ×g for 30 min for morphological observation by scanning electron microscopy (SEM) (Hitachi SU8100, Tokyo, Japan). The remaining cultures were incubated for an additional 8 hours. Minicells were isolated through a series of centrifugation and filtration steps. The majority of bacterial cells were removed via low-speed centrifugation at 3000 ×g for 15 min. The resulting supernatant was then centrifuged at 13000 ×g for 30 min to obtain a crude minicell fraction. To eliminate residual whole bacteria, the pellet was resuspended in 300 mL of fresh LB medium containing 100 μg/mL ceftriaxone and cultured at 37°C at 220 rpm for 2 hours. The suspension was then centrifuged at 3000 ×g for 15 min, and the supernatant was collected after centrifugation at 13000 ×g for 30 min to harvest the purified minicells. The final minicell pellet was washed with 300 mL of phosphate-buffered saline (PBS), collected by centrifugation,

resuspended in 100 mL of PBS, and sequentially filtered through 0.65 μm and 0.45μm membranes. Finally, the resulting purified minicells were resuspended in 500 μL of PBS. Throughout the process, samples were taken at the designated key stages, examined via oil-immersion microscopy, and plated on LB agar plates to monitor bacterial contamination. Minicell identity was further verified via nanoparticle tracking analysis (NTA) and transmission electron microscopy (TEM), which were performed by MISP Biotechnology Corporation (Wuhan, China).

Construction of expression plasmids with different translational strengths

The plasmids used in this study are listed in Table 1. All constructs were engineered using standard molecular biology techniques. The expression of eGFP was placed under the control of a *Lac* promoter, with the ribosomal binding sites (RBS) being systematically varied. The pUC19-eGFP plasmid, which was commercially sourced from Genecarer (Xi'an, China), served as the parental backbone. The derivative plasmids, pUC19-OmpA-eGFP and pUC19-J61100-eGFP, were constructed by excising the native sequence (which may have contained a rbs) from the parent plasmid with *Hind III* and *Kpn I* restriction enzymes and replacing it with synthetic DNA fragments containing OmpA rbs or J61100 rbs (from the Anderson RBS library), respectively[30-32]. All plasmid sequences were synthesized and verified by Genecarer Biotechnology Corporation (Xi'an, China). The specific replaced sequences and the engineered RBS sequences are detailed in Table S2 of the Supplementary Material.

Expression of recombinant eGFP in ΔEcN

The ΔEcN cells were separately transformed with the pUC19-eGFP, pUC19-OmpA-eGFP, or pUC19-J61100-eGFP plamids. Positive monoclonal transformants were selected and cultured overnight at 37°C in LB liquid media supplemented with 50 μg/mL kanamycin and 100 μg/mL ampicillin. This overnight culture was then diluted 1:100 (v/v) in 100mL of fresh medium and incubated at 37°C with shaking at 220 rpm. Once the OD_{600} reached approximately 0.6–0.8, 0.2 mM isopropyl β-D-thiogalactoside (IPTG) was added to induce eGFP expression at 28°C. Bacterial growth curves were plotted with the parental ΔEcN strain as the control to assess the impact of recombinant protein expression on cell growth. To determine the optimal induction time, ΔEcN cells harboring the different plasmids were harvested by centrifugation (13000 × g, 30 min) at 0.5, 2, 4 and 6 h after induction. The pellets were resuspended in PBS for subsequent analysis. eGFP expression levels driven by different RBSs were evaluated by fluorescence intensity and further confirmed by Western blot analysis. Additionally, at the selected optimal time point, bacterial viability was qualitatively assessed using the SYTO9/PI Live/Dead Bacterial Stain Kit (Bingene, China) according to the manufacturer's protocol, and eGFP expression was visualized by fluorescence microscopy (DM3000, Leica, Germany).

Expression of recombinant eGFP in minicells

The minicells were harvested at the optimal time point (6 h after induction) for eGFP expression. The minicells, which were purified from a 1 L culture, were resuspended in 500 μL of PBS. The concentration of the minicells was determined by measuring the optical density at 600 nm (OD_{600}). The integrity of

minicells was assessed using a SYTO9/PI Live/Dead Bacterial Stain kit. The total protein concentration in both bacterial cells and minicells was determined using a bicinchoninic acid (BCA) assay kit (Beyotime, China).

Fluorescence intensity detection

Samples equivalent to 0.1 OD_{600} unit of bacterial cells or 0.05 OD_{600} unit of minicells were washed and resuspended in 50 μL of PBS. Following lysis in bacterial lysis buffer and centrifugation at 13000 × g for 30 min, the resulting supernatant was added to the microplate. The fluorescence intensity was then measured using a Thermo Scientific™ Varioskan™ LUX microplate reader (with excitation at 488 nm and emission at 507 nm).

Western Blot detection

The cell pellets corresponding to either 0.1 OD_{600} unit of bacterial cells or 0.02 OD_{600} unit of minicells were resuspended in 20 μL of PBS, mixed with 5× loading buffer and boiled for 10 min. The denatured samples were separated by 12% SDS-PAGE and subsequently transferred onto a polyvinylidene fluoride (PVDF) membrane. The membrane was then processed for immunoblotting according to a standard protocol. Briefly, the PVDF membrane was blocked with 5% skim milk and then incubated successively with primary antibody (mouse anti-eGFP antibody, F56-6A1.2.3, Invitrogen, USA) and secondary antibody (HRP-conjugated goat anti-mouse IgG, D110087, Sangon, China). Each experiment was performed in at least three independent biological replicates. The protein bands were visualized using a gel imaging system (Shenhua, China) and analysed with ImageJ software.

Detection of soluble proteins

A 0.1 OD_{600} unit of bacterial cells was resuspended in 20 μL of PBS. After lysis and centrifugation at 13000 ×g for 30 min, the supernatant and the precipitate were resuspended in an equal volume of PBS and assayed via Western blotting. Notably, for the scarce minicell samples (0.02 OD_{600} unit/20 μL of PBS), soluble eGFP expression was evaluated on the basis of fluorescence intensity to preserve the samples for further Western blot detection.

Statistical analysis

Statistical analysis was performed using GraphPad Prism software. Data are expressed as the mean ± standard deviation (SD), and significance among groups was determined by one-way or two-way analysis of variance (ANOVA), where $P < 0.05$ was considered statistically significant.

Results

Construction of an engineered strain of E.coli for generating minicells

The EcN strain was genetically engineered using λ Red-mediated homologous recombination to enable minicell generation (Fig. 1A). Successful deletion of the *minCD* gene was confirmed by agarose gel electrophoresis (Fig. 1B) and DNA sequencing (Fig. 1D). The resulting mutant strain was designated ΔEcN. Minicells produced by ΔEcN were initially observed by bright-field (BF) microscopy and hematoxylin–eosin (HE) staining (Fig. 1E). Their formation was further clearly visualized by scanning electron microscopy, which captured the budding process of minicells (Fig. 1F). While the engineered ΔEcN strain showed increased cell length (2.5–7 μm) compared with the original EcN strain (1.5–3 μm), its growth profile was not significantly altered (Fig. 1C), indicating that ΔEcN is suitable as an engineered strain for subsequent studies.

Minicells were isolated from parental ΔEcN cells through a combination of repeated centrifugation and filtration (Fig. 2A). During this process, samples were collected at five key steps: before extraction, before and after ceftriaxone addition, and before and after filtration. As shown in Fig. 2B, whole bacteria and their reproductive forms were completely removed through this process. Ultimately, a high yield of purified minicells was obtained (Fig. 2D), with particle sizes predominantly ranging from 100 to 200 nm (Fig. 2C). These results demonstrate that highly purified minicells can be efficiently obtained using this production system.

Effects of different RBSs on recombinant eGFP expression

To achieve precise regulation of recombinant protein expression, we modulated translation efficiency by altering the RBS while keeping the promoter constant. Since the RBS controlling eGFP expression in the plasmid pUC19-eGFP was undefined, we hypothesized that the region 7–40 bp located upstream of the eGFP start codon might harbor a functional RBS. We therefore replaced this region with two previously reported RBS sequences, OmpA-RBS and J61100-RBS (Fig. 3A). The new plasmids obtained were named pUC19-OmpA-eGFP and pUC19-J61100-eGFP, respectively (Table 1).

Each plasmid was subsequently transformed into ΔEcN cells. Using plasmid-free ΔEcN as a control, we examined the effect of recombinant protein expression on bacterial growth by monitoring growth curves. As shown in Fig. 3B, all four strains reached the logarithmic growth phase approximately three hours after subculturing from an overnight suspension. At this time point, IPTG was added to induce recombinant eGFP expression. eGFP expression levels were subsequently quantified by western blot and fluorescence intensity measurements. The results showed that Lac-eGFP (from pUC19-eGFP) exhibited the highest expression, followed by J61100-eGFP (from pUC19-J61100-eGFP), whereas OmpA-eGFP (from pUC19-OmpA-eGFP) showed the weakest expression (Figs. 3C and 3E). Furthermore, on the basis of the above statistical data, cultivation was terminated after 6 h of induction to achieve optimal concurrent production of eGFP and minicells.

Following the 6 h induction, a series of subsequent experiments were performed. As expected, the progressively increasing fluorescence intensity of eGFP expressed under different RBS regulations was confirmed by fluorescence microscopy (Fig. 3D) and was also visually observable (Fig. 3H). This finding

correlated well with the western blot and quantitative analyses. To further investigate the effects of RBS variants on bacterial physiology, soluble eGFP expression and bacterial viability were evaluated. The percent solubility (soluble/total protein) of Lac-eGFP (69%) was lower than that of J61100-eGFP (73%) and OmpA-eGFP (91%) (Fig. 3F), suggesting that higher target-protein expression in this system tended to correspond with lower solubility. Additionally, the viability of eGFP-expressing strains was generally lower than that of the empty-vector control strain(Fig. 3G). Notably, the viability of the strain with OmpA-eGFP expression was slightly greater than that of the other two higher-expression groups, although the difference was relatively modest. These results demonstrate that varying the RBS sequence significantly affects both the expression level and solubility of eGFP, whereas its impact on bacterial viability is limited. This finding eliminates potential confounding background factors, thereby enabling a more focused investigation into the relationship between the expression of target protein and minicell generation.

Relationship between target protein production and minicell generation

Minicells from 1 L of induced bacterial cultures were purified by centrifugation and filtration. The minicell pellets from each of the four groups were resuspended in 500 µL of PBS, yielding plasmid-free minicells (OD_{600} = 0.1551), followed by minicells expressing OmpA-eGFP (OD_{600} = 0.1074), J61100-eGFP (OD_{600} = 0.1016), and Lac-eGFP (OD_{600} = 0.0986). These results suggest that higher expression of the target protein is associated with lower minicell yields. However, no significant difference in minicell integrity was observed among the groups, supporting the use of consistent extraction procedures across all the samples (Fig. 4A).

We further examined eGFP expression in the harvested minicells. On a per-unit basis, minicells accumulated more total protein as well as more target protein than whole bacterial cells (Fig. 4B and 4C), which is consistent with previous reports [8, 33]. It is worth noting that the soluble expression levels of Lac-eGFP (92%) and J61100-eGFP (86%) were greater in minicells than in bacteria cells, whereas the opposite trend was observed for OmpA-eGFP (81%) (Fig. 3F and 4D). Importantly, the relative expression trends of eGFP driven by different RBS sequences remained consistent between minicells and their parental bacteria (Fig. 4C and 4D). These expression patterns were also visualized by fluorescence confocal microscopy (Fig. 4E).

Discussion

In this study, we systematically investigated the interplay between recombinant protein expression and minicell biogenesis in *Escherichia coli* by employing RBS sequence engineering as a precise strategy for translational control. Our findings revealed a clear trade-off: high-level expression of the model protein eGFP was correlated with a significant decrease in minicell yield. This inverse relationship likely stems from the substantial metabolic burden imposed by the synthesis of heterologous proteins, which compete with the cellular resources essential for growth and proper cell division, including minicell

formation [21]. This observation contrasts with some prior minicell studies that did not report such a yield penalty, possibly due to differences in protein identity, induction strength, or the specific genetic backgrounds used [9].

A key and promising finding of our work is the superior protein folding environment within minicells. Notably, the solubilities of Lac-eGFP and J61100-eGFP were markedly greater in minicells than in whole bacterial cells. This enhancement suggests that minicells, which are devoid of chromosomes, may offer a favourable environment for recombinant protein folding. Potential factors include a limited proteolytic system, or a less crowded cytoplasmic environment[9]. The exceptional behaviour of OmpA-eGFP may be explained by its different RBS characteristics or unstable low-level expression, potentially increasing its susceptibility to aggregation or misfolding in minicells. This protein-specific behaviour highlights the need for case-by-case optimization.

Interestingly, although the RBS region of the pUC19-eGFP plasmid is not clearly defined, we obtained an expression hierarchy (Lac-eGFP > J61100-eGFP > OmpA-eGFP) by replacing the other two RBS sequences. This indirectly indicates that the original sequence that was replaced likely contained an RBS. Importantly, this characteristic of expression differences was faithfully preserved not only in soluble protein levels within parent bacteria but also in the total and soluble protein contents loaded into minicells. This consistency confirms that translational regulation via RBS design is a robust and transferable principle for tuning protein encapsulation in minicells.

In conclusion, by linking RBS strength to minicell yield and functionality, our study provides a rational design strategy for engineering next-generation minicell-based therapeutic nanocarriers and enzymatic bioreactors. These findings against the simplistic pursuit of maximal target protein expression, as this can diminish the nanoparticle yield, which is a critical parameter for applications. Instead, an optimal balance must be struck. Future work should focus on elucidating the precise molecular mechanisms linking metabolic load to division site errors in minicell-generating strains.

Abbreviations

Abbreviation	Full title
EcN	*Escherichia coli* Nissle 1917
RBS	ribosome-binding site
eGFP	enhanced green fluorescent protein

Declarations

Ethics approval and consent to participate

Not applicable

Consent for publication

Not applicable

Availability of data and materials

All data generated or analysed during this study are included in this published article [and its supplementary information files].

Competing interests

The authors declare that they have no competing interests.

Funding

Funding for this work was provided by Natural Science Foundation of Shaanxi Province in China (Grant No. 2023-JC-QN-0966) and Science and Technology Bureau of Xi'an in China (Grant No. 24YXYJ0201).

Authors' contributions

YR and JY conceived the study. YR, YN, TL, XS, MZ and SL performed the experiments and analysed the data. YR and HX analysed the data and wrote the manuscript. All authors contributed to manuscript revision, read, and approved the submitted version.

Acknowledgments

Not applicable

References

1. Abdessalem MA, Adham SA. Research advancements in nanoparticles and cell-based drug delivery systems for the targeted killing of cancer cells. Oncol Res. 2025;33:27–44. https://doi.org/10.32604/or.2024.056955.
2. Ma X, Tian Y, Yang R, Wang H, Allahou LW, Chang J, et al. Nanotechnology in healthcare, and its safety and environmental risks. J Nanobiotechnol. 2024;22:715. https://doi.org/10.1186/s12951-024-02901-x.
3. Ren H, Jia W, Xie Y, Yu M, Chen Y. Adjuvant physiochemistry and advanced nanotechnology for vaccine development. Chem Soc Rev. 2023;52:5172–254. https://doi.org/10.1039/D2CS00848C.
4. Haidar LL, Bilek M, Akhavan B. Surface bio-engineered polymeric nanoparticles. Small Weinh Bergstr Ger. 2024;20:e2310876. https://doi.org/10.1002/smll.202310876.
5. Ali M. What function of nanoparticles is the primary factor for their hyper-toxicity? Adv Colloid Interface Sci. 2023;314:102881. https://doi.org/10.1016/j.cis.2023.102881.

6. Dutt Y, Pandey RP, Dutt M, Gupta A, Vibhuti A, Vidic J, et al. Therapeutic applications of nanobiotechnology. J Nanobiotechnol. 2023;21:148. https://doi.org/10.1186/s12951-023-01909-z.
7. Ali MK, Liu Q, Liang K, Li P, Kong Q. Bacteria-derived minicells for cancer therapy. Cancer Lett. 2020;491:11–21. https://doi.org/10.1016/j.canlet.2020.07.024.
8. Valenzuela-Ibaceta F, Torres-Olea N, Ramos-Zúñiga J, Dietz-Vargas C, Navarro CA, Pérez-Donoso JM. Minicells as an escherichia coli mechanism for the accumulation and disposal of fluorescent cadmium sulphide nanoparticles. J Nanobiotechnol. 2024;22:78. https://doi.org/10.1186/s12951-024-02348-0.
9. Zhang D, Liao J, He S, Wang M, Chen J, Chen Y, et al. Advances in production and application technologies of minicells: a review. Biotechnol Adv. 2025;83:108648. https://doi.org/10.1016/j.biotechadv.2025.108648.
10. MacDiarmid JA, Brahmbhatt H. Minicells: versatile vectors for targeted drug or si/shRNA cancer therapy. Curr Opin Biotechnol. 2011;22:909–16. https://doi.org/10.1016/j.copbio.2011.04.008.
11. Solomon BJ, Desai J, Rosenthal M, McArthur GA, Pattison ST, Pattison SL et al. A first-time-In-human phase I clinical trial of bispecific antibody-targeted, paclitaxel-packaged bacterial minicells. Rosell R, editor. PLOS One. 2015;10:e0144559. https://doi.org/10.1371/journal.pone.0144559
12. Adler HI, Fisher WD, Cohen A, Hardigree AA. MINIATURE escherichia coli CELLS DEFICIENT IN DNA. Proc Natl Acad Sci U S A. 1967;57:321–6. https://doi.org/10.1073/pnas.57.2.321.
13. Kim S-J, Chang W, Oh M-K. Escherichia coli minicells with targeted enzymes as bioreactors for producing toxic compounds. Metab Eng. 2022;73:214–24. https://doi.org/10.1016/j.ymben.2022.08.006.
14. Yu H, Khokhlatchev AV, Chew C, Illendula A, Conaway M, Dryden K, et al. Minicells from highly genome reduced *escherichia coli*: cytoplasmic and surface expression of recombinant proteins and incorporation in the minicells. ACS Synth Biol. 2021;10:2465–77. https://doi.org/10.1021/acssynbio.1c00375.
15. Zhang Y, Ji W, He L, Chen Y, Ding X, Sun Y, et al. E. coli nissle 1917-derived minicells for targeted delivery of chemotherapeutic drug to hypoxic regions for cancer therapy. Theranostics. 2018;8:1690–705. https://doi.org/10.7150/thno.21575.
16. Chen H, Lei P, Ji H, Yang Q, Peng B, Ma J, et al. Advances in escherichia coli nissle 1917 as a customizable drug delivery system for disease treatment and diagnosis strategies. Mater Today Bio. 2023;18:100543. https://doi.org/10.1016/j.mtbio.2023.100543.
17. Lynch JP, Goers L, Lesser CF. Emerging strategies for engineering escherichia coli nissle 1917-based therapeutics. Trends Pharmacol Sci. 2022;43:772–86. https://doi.org/10.1016/j.tips.2022.02.002.
18. Redenti A, Im J, Redenti B, Li F, Rouanne M, Sheng Z, et al. Probiotic neoantigen delivery vectors for precision cancer immunotherapy. Nature. 2024;635:453–61. https://doi.org/10.1038/s41586-024-08033-4.
19. Ma Y, Zhu G, Feng L, Jiang S, Xiang Q, Wang J. Efficient cytotoxicity of recombinant azurin in escherichia coli nissle 1917-derived minicells against colon cancer cells. Bioengineering.

2023;10:1188. https://doi.org/10.3390/bioengineering10101188.

20. Yu M, Hu S, Tang B, Yang H, Sun D. Engineering escherichia coli nissle 1917 as a microbial chassis for therapeutic and industrial applications. Biotechnol Adv. 2023;67:108202. https://doi.org/10.1016/j.biotechadv.2023.108202.
21. Snoeck S, Guidi C, De Mey M. Metabolic burden explained: stress symptoms and its related responses induced by (over)expression of (heterologous) proteins in escherichia coli. Microb Cell Factories. 2024;23:96. https://doi.org/10.1186/s12934-024-02370-9.
22. Xu N, Wei L, Liu J. Recent advances in the applications of promoter engineering for the optimization of metabolite biosynthesis. World J Microbiol Biotechnol. 2019;35:33. https://doi.org/10.1007/s11274-019-2606-0.
23. Chizzolini F, Forlin M, Yeh Martín N, Berloffa G, Cecchi D, Mansy SS. Cell-free translation is more variable than transcription. ACS Synth Biol. 2017;6:638–47. https://doi.org/10.1021/acssynbio.6b00250.
24. Liu M, Jin Z, Xiang Q, He H, Huang Y, Long M, et al. Rational design of untranslated regions to enhance gene expression. J Mol Biol. 2024;436:168804. https://doi.org/10.1016/j.jmb.2024.168804.
25. Zhang Y, Chen H, Zhang Y, Yin H, Zhou C, Wang Y. Direct RBS engineering of the biosynthetic gene cluster for efficient productivity of violaceins in E. coli. Microb Cell Factories. 2021;20:38. https://doi.org/10.1186/s12934-021-01518-1.
26. de Boer PA, Crossley RE, Rothfield LI. A division inhibitor and a topological specificity factor coded for by the minicell locus determine proper placement of the division septum in E. coli. Cell. 1989;56:641–9. https://doi.org/10.1016/0092-8674(89)90586-2.
27. Corts A, Thomason LC, Costantino N, Court DL. Recombineering in non-model bacteria. Curr Protoc. 2022;2:e605. https://doi.org/10.1002/cpz1.605.
28. Rangarajan AA, Yilmaz C, Schnetz K. Deletion of FRT-sites by no-SCAR recombineering in escherichia coli. Microbiol Read Engl. 2022;168. https://doi.org/10.1099/mic.0.001173.
29. Green MR, Sambrook J. Nested polymerase chain reaction (PCR). Cold Spring Harb Protoc. 2019;2019. https://doi.org/10.1101/pdb.prot095182
30. Anderson RBSlibrary. Part:BBa J61100 - parts.igem.org. Accessed 7 June 2025.
31. Larsson EM, Wang OY, Murray RM. A DNA part library for reliable engineering of the emerging model nematode symbiotic bacterium *xenorhabdus griffiniae* HGB2511. ACS Synth Biol. 2025;14:4122–6. https://doi.org/10.1021/acssynbio.5c00414.
32. Zhu J, Ruan Y, Fu X, Zhang L, Ge G, Wall JG, et al. An engineered pathway for production of terminally sialylated N-glycoproteins in the periplasm of escherichia coli. Front Bioeng Biotechnol. 2020;8:313. https://doi.org/10.3389/fbioe.2020.00313.
33. Park J, Polizzi KM, Kim J, Kim J. Manipulating subcellular protein localization to enhance target protein accumulation in minicells. J Biol Eng. 2025;19:27. https://doi.org/10.1186/s13036-025-00495-y.

Figures

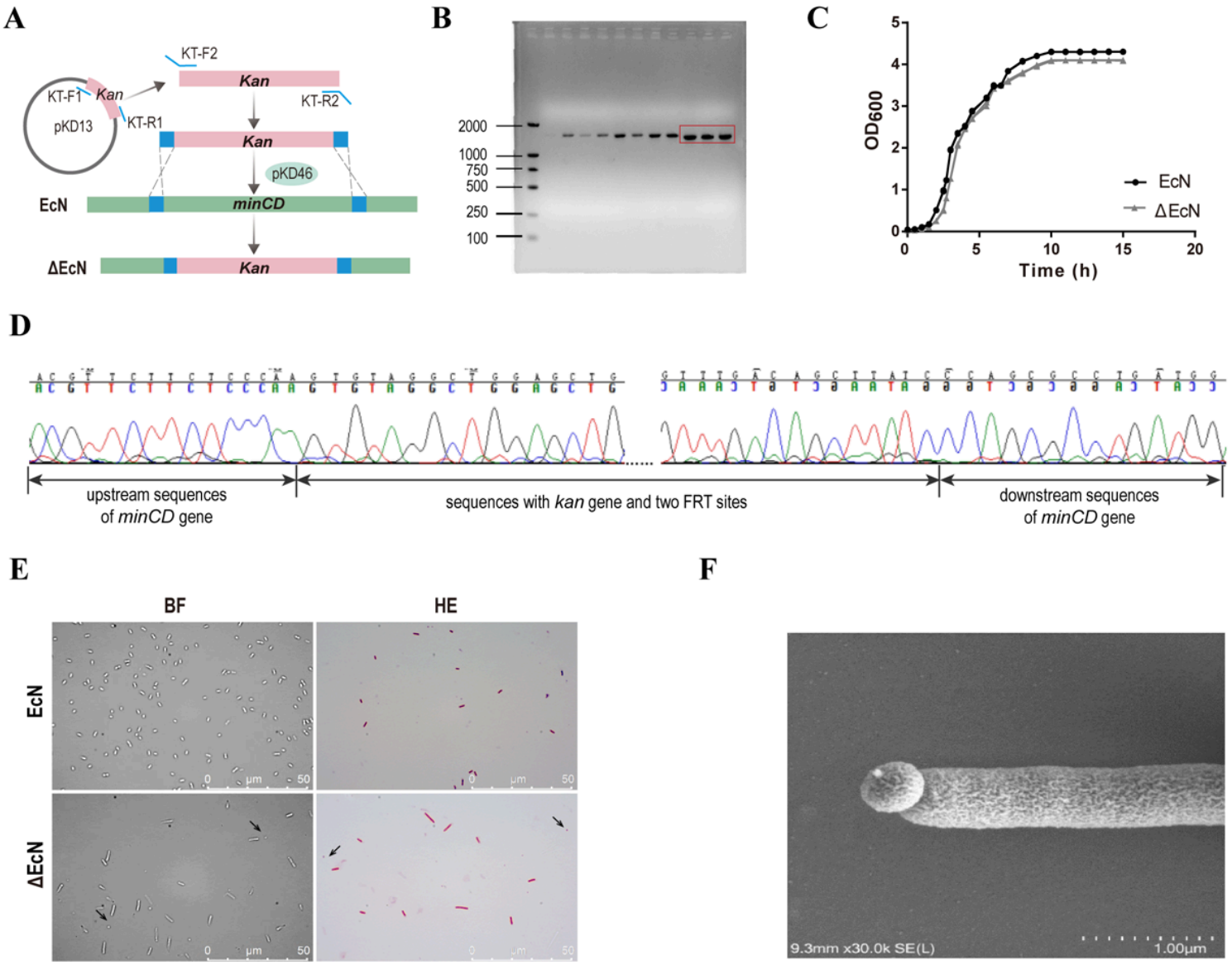


Figure 1

Construction and characterization of ΔEcN for generating minicells. (A) Deletion of the *minCD* gene using λ Red-mediated homologous recombination. (B) Verification of the deletion of the *minCD* gene by agarose gel electrophoresis. The three strains with successful gene knockouts (1496 bp) are indicated within the red boxes, whereas the eight strains that failed the knockout process (1527 bp) are shown outside the boxes. Maker: DL 2000 DNA maker (Sangon, China). (C) Growth curves of EcN and ΔEcN. (D) Gene sequencing of DNA fragments lacking the *minCD*gene. (E) Comparison of EcN and ΔEcN by bright-field (BF) microscopy and hematoxylin–eosin (HE) staining. The minicells (black arrow) can be observed in the ΔEcN group. (F) Observation of the budding of the minicell from ΔEcN as seen using scanning electron microscopy.

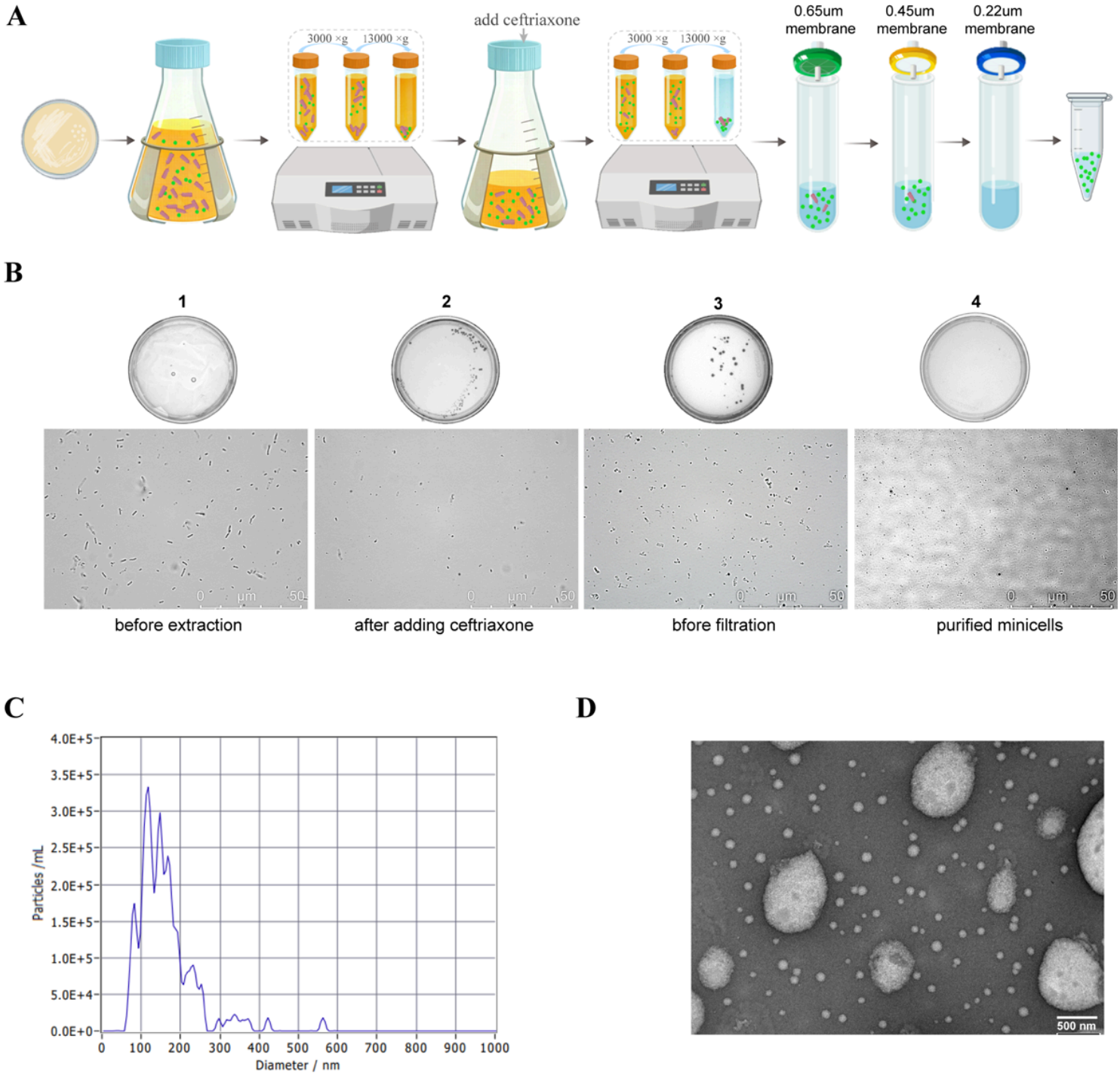


Figure 2

Purification of minicells from ΔEcN. (A) Schematic illustration depicting the purification of minicells from patental ΔEcN. (B) Observation of elimination of bacteria and their reproductive forms through microscopes (lower panel) and bacterial cultures (upper panel) during the process of minicell extraction. 1: before extraction, 2: after adding ceftriaxone, 3: before filtration, 4: purified minicells resuspended in 500 μL of PBS. (C) Nanoparticle tracking analysis of purified minicells. (D) Observation of purified minicells using transmission electron microscopy.

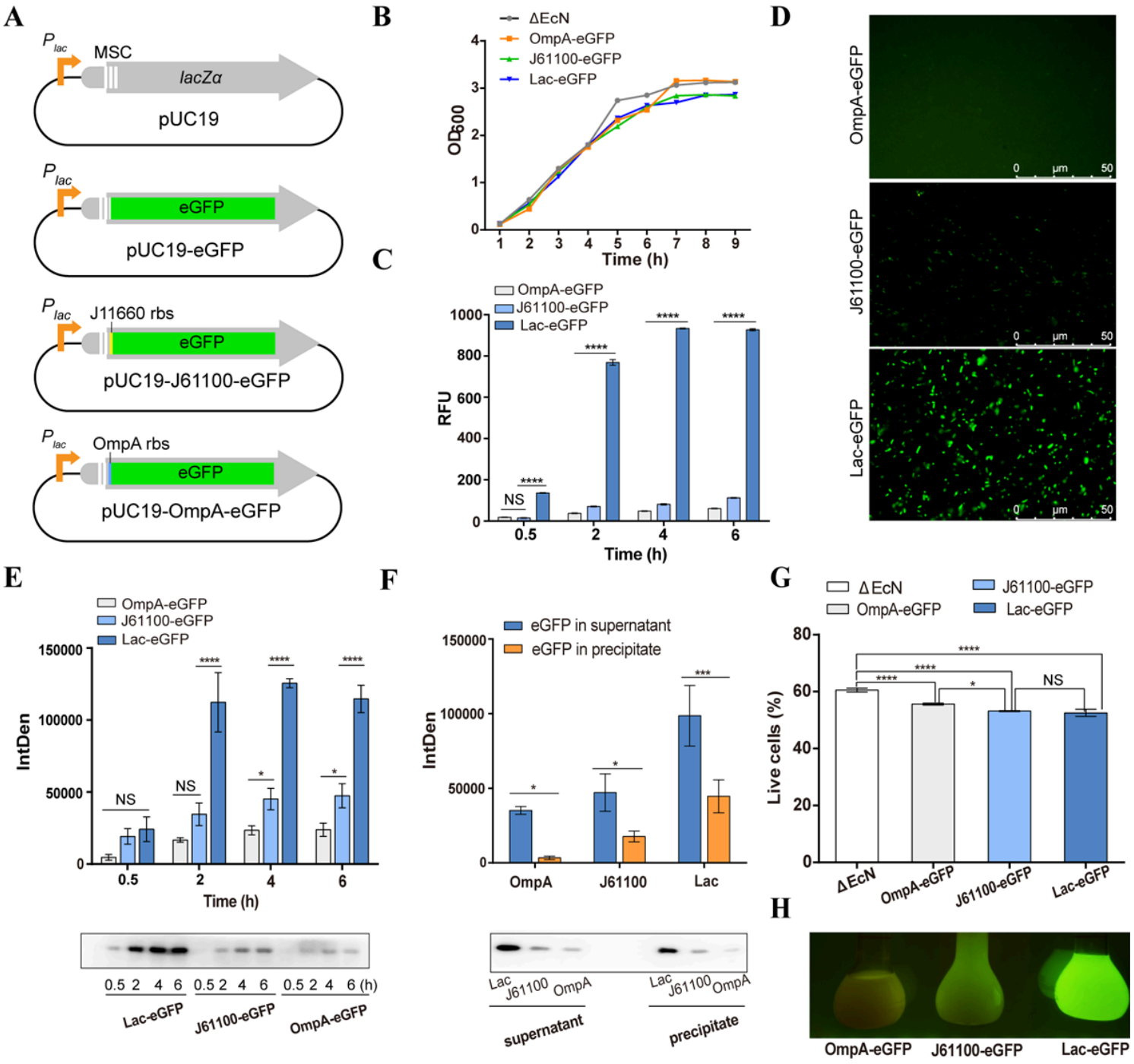


Figure 3

Construction of expression plasmids with different translational strengths by RBS mutant. (A) Diagram of the pUC19-eGFP, pUC19-J61100-eGFP and pUC19-OmpA-eGFP plasmids. (B) Growth curves of ΔEcN and ΔEcN with plasmids pUC19-OmpA-eGFP (OmpA -eGFP), ΔEcN/pUC19-J61100-eGFP (J61100-eGFP) or ΔEcN/pUC19-eGFP (Lac-eGFP). Detection of eGFP protein in ΔEcN with above different plasmids by fluorescence intensity (C), fluorescence microscopy (D) and western blotting (E). (F) Detection of eGFP in supernatant and precipitate of ΔEcN with different plasmids by western blotting. (G) Assessment of bacterial viability of ΔEcN and ΔEcN with different plasmids. (H) Fluorescence intensity under the naked eye of eGFP in ΔEcN with above different plasmids. NS, P>0.05; *P<0.05, ***P<0.001, ****P<0.0001.

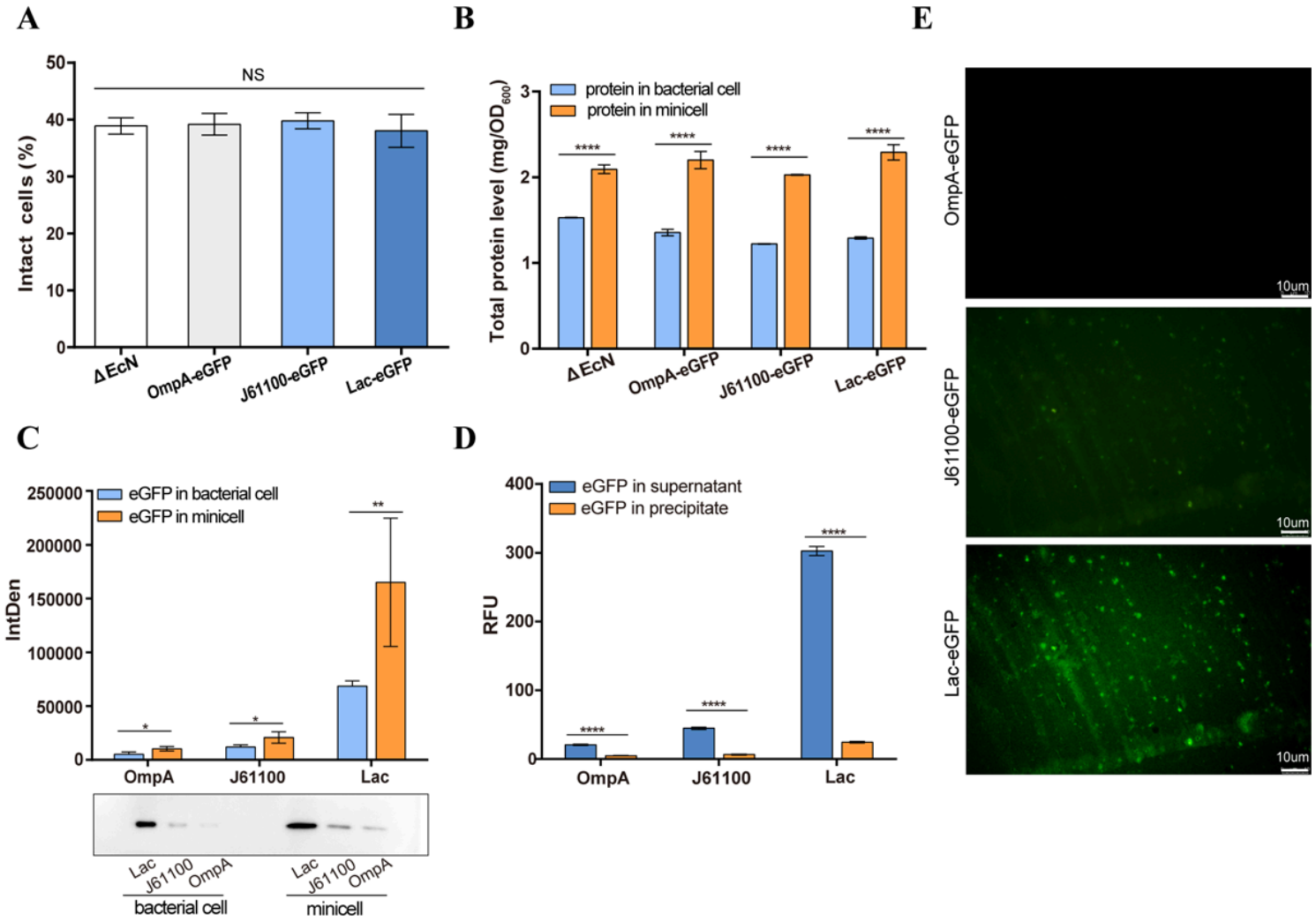


Figure 4

Assesment of expression of eGFP under different RBSs in minicell. (A) Assessment of integrity of minicells from ΔEcN and ΔEcN/pUC19-OmpA-eGFP (OmpA-eGFP), ΔEcN/pUC19-J61100-eGFP (J61100-eGFP) or ΔEcN/pUC19-eGFP (Lac-eGFP). (B) Detection of total protein in whole bacterial cells or minicells by BCA assay. (C) Detection of eGFP protein in whole bacterial cells or minicells by western blotting. (D) Analysis of eGFP in supernatant and precipitate of minicells from ΔEcN with different plasmids by fluorescence intensity. (E) Detection of eGFP protein in minicells from ΔEcN with different plasmids by fluorescence microscopy. *P<0.05, **P<0.01, ****P<0.0001.

Supplementary Files

This is a list of supplementary files associated with this preprint. Click to download.

- SupplementaryMaterial.docx
- supplementaryfileOriginalBlotsimages.docx